Int J Adv Manuf Technol (2016) 84:2391–2399
DOI 10.1007/s00170-015-7904-6

ORIGINAL ARTICLE

Investigation of vertical compensation friction stir-welded 7N01-T4 aluminum alloy

S. D. Ji[1] · X. C. Meng[1] · Z. W. Li[1] · L. Ma[1] · S. S. Gao[1]

Received: 22 May 2015 / Accepted: 24 September 2015 / Published online: 1 October 2015

Abstract Vertical compensation friction stir welding (VCFSW) is successfully applied to weld 7N01-T4 aluminum alloy, and effects of welding speed on joint quality are investigated. The results show that when compensation strip width is 1 mm, the defect-free joint is obtained at the welding speed of 50 mm/min and constant rotational velocity of 2000 rpm. Moreover, the intercalation lamellae structure formed in nugget zone (NZ) can reveal material flow behavior clearly. As strip width increases to 1.5 mm, it is difficult to attain sound joint. Decreasing welding speed is beneficial to surface formation of VCFSW joint. The increase of welding speed decreases tensile strength and elongation of joint. At the welding speed of 50 mm/min and strip width of 1 mm, the tensile strength and elongation of VCFSW joint are 295.7 MPa and 6.7 %, equivalent to 66 and 39.4 % of BM, respectively, while fracture surface of joint presents typical ductile fracture. The hardness distribution of joint shows typical W shape, and the hardness of NZ exhibits uniform distribution.

Keywords Vertical compensation friction stir welding · 7N01-T4 aluminum alloy · Gap · Surface formation · Mechanical property

✉ S. D. Ji
superjsd@163.com

[1] Faculty of Aerospace Engineering, Shenyang Aerospace University, No.37 Daoyi South Avenue, Daoyi Development District, Shenyang 110136, China

1 Introduction

Friction stir welding (FSW), as a mature solid-state welding technique, was developed and patented by The Welding Institute (TWI) in Camridge, UK, in 1991 [1]. Compared with fusion welding, FSW owns many advantages such as high joint strength, low distortion, no cracks, low power consumption, and non-pollution [2–4]. Therefore, FSW has been widely applied in aerospace, automotive, electronics, and shipbuilding. However, during FSW process, formation of joint is affected by many various factors, which may produce tunnel and groove defects, degrading mechanical properties [1, 5]. Although rational rotational tool and welding parameters can avoid the occurrence of defect, it always wastes amounts of materials and time for research [6]. Therefore, many researchers at home and abroad have proposed some methods to eliminate FSW defects [7–10]. Liu et al. [7] used FSW to repair groove defect and demonstrated that appropriate tool offset was beneficial to obtain repaired joint with high quality. Yao et al. [8] also combined TIG welding with FSW to repair tunnel defect of FSW joint.

In fact, the formation of tunnel and groove defects of FSW joint results in the loss of material. During the repairing of defect process, if no material is added into the groove or tunnel, it easily leads to thickness reduction and then decreases the ability of loading bearing, deteriorating mechanical properties. Besides the groove and tunnel defects, a gap before welding at the interface between two workpieces, resulted from the extrusion effect of FSW or accumulation of some manufacturing errors of large structures, cannot be neglected, which always leads to the reduction of joint quality [11–16]. Seidel et al. [11] found that the occurrence of gap could not only make plasticized materials flow into gap resulting in the loss of materials and then produces the lack of root penetration but also lead to thickness reduction of joint. Yang et al. [14],

Wanjara et al. [15], and Shultz et al. [16] also investigated the effect of gap during FSW process and expounded that a gap could lead to the decrease of effective contact area or appearance of wormhole, fabricating an unsuitable weld.

Therefore, in order to eliminate the adverse effect caused by gap, tunnel, or groove defect, a vertical compensation friction stir welding (VCFSW) method has been put forward by Ji and Meng et al. [17]. We found that choosing 6061-T6 aluminum alloy as research object, VCFSW assisted by stationary shoulder tool could effectively eliminate the adverse effect induced by gap. As one of high-strength aluminum alloys, 7N01 aluminum alloy is widely applied in high-speed train because of high-strength, good corrosion resistance, and weldability. However, when using fusion welding to weld 7N01 aluminum alloy, hot crack, porosity, and lack of fusion defects easily appear in the joint, which restrict the wide application of 7N01 aluminum alloy [18, 19]. In this study, employing a common rotational tool, VCFSW experiments of 7N01-T4 aluminum alloy were carried out, which has profound significance for wide application of 7N01 and development of VCFSW. Furthermore, effects of welding speed on formation, microstructures, and mechanical properties of VCFSW joint were investigated in details.

2 Experimental procedure

The base material (BM) used in this experiment was a 4-mm-thick 7N01-T4 aluminum alloy plate, while the nominal chemical composition of BM is shown in Table 1. Meanwhile, a strip of aluminum alloy was selected as compensation material, which was added into the gap between two workpieces to be welded, as shown in Fig. 1. In our pre-experiment, it was found that when compensation material was same as BM, it was difficult to avoid the lack of root penetration because the section of compensation strip near the bottom of workpiece was impossible to be thoroughly broken into pieces and mixed with BM as a result of lower temperature [17]. Therefore, 2024-T4 aluminum alloy owning lower solidus temperature compared with 7N01 aluminum alloy was selected as compensation material, whose nominal chemical composition of 2024-T4 aluminum alloy is indicated in Table 1. Rotational tool used in this study is made of H13 tool steel, which consists of concentric-circles-flute shoulder of 14 mm diameter and right-screwed pin of 3.8 mm length. The diameters of pin bottom and tip are 5 and 3 mm, respectively. The close-up

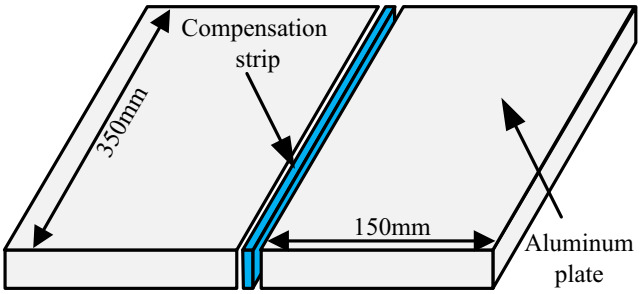

Fig. 1 Schematic diagram of VCFSW process

photograph of rotational tool is exhibited in Fig. 2. In the experiment, the rotational tool rotates anti-clockwise and the tilt angle with respect to *z*-axis is 2.5°. In this study, welding speed varies from 50 to 300 mm/min, while rotational velocity of 2000 rpm remains constant. Before welding, BM and compensation strip to be welded were burnished by abrasive paper and cleaned using acetone in order to wipe off oxide layer.

After welding, the specimens were cut perpendicular to the welding direction by an electrical discharge cutting machine to perform the mechanical test and microstructural characterization. The microstructural features were observed by an optical microscopy (OLYMPUS, GX71) after etched by Keller's reagent. To evaluate mechanical property of VCFSW joint, three tensile specimens were fabricated for each joint with reference to GB/T 2651-2008 (equivalent to ISO 9016: 2001) and the average value was presented for discussion [20]. Furthermore, tensile test at room temperature was carried out at a constant crosshead speed of 5 mm/min. Microhardness of VCFSW joint was measured by a microhardness tester at a load of 200 g for 10 s under a constant interval of 0.5 mm. Fracture surface of tensile specimen was observed by a scanning electron microscopy (SEM, KYKY-2800B). Elemental analysis of the cross section characteristic of VCFSW joint was performed by SEM equipped with an energy-dispersive X-ray spectroscopy (EDX).

3 Results and discussion

3.1 Formation of joint

Figure 3 exhibits the surface formation of joints produced by different welding process parameters. During traditional FSW process, the occurrence of gap decreases the effective contact area between rotational tool and BM, leading to inadequate

Table 1 Nominal chemical compositions of 7N01 alloy and 2024 alloy (mass fraction, %)

Alloy	Si	Fe	Cu	Mn	Mg	Cr	Zn	Ti	Al
7N01	0.3	0.35	0.2	0.2~0.7	1.0~2.0	0.3	4.0~5.0	0.2	Balance
2024	0.50	0.50	3.8~4.9	0.30~0.9	1.2~1.8	–	0.25	0.15	Balance

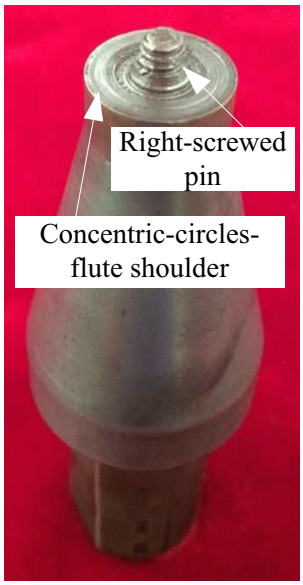

Fig. 2 Rotational tool used in this experiment

frictional heat [14–16]. Because 7N01 alloy belongs to high-strength aluminum alloy, insufficient frictional heat results in big flow stress and then causes worse material flow behavior. In addition, the appearance of gap also makes more plasticized material flow into the gap so that nugget zone (NZ) is difficult to be filled with material. Therefore, the groove defect easily appears in the NZ under the conditions of the gap of 1 mm and no compensation strip, as indicated in Fig. 3a. In addition, because forging pressure cannot be controlled for displacement-controlled FSW machine used in this study, the decrease of forging force caused by gap is also detrimental to the formation of joint [17].

In order to eliminate the adverse effect generated by gap, a compensation strip is added into the gap and the partial magnified pictures of joints under the strip width of 1 mm and different welding speeds are shown in Fig. 3b–f. When the welding speed is 50 mm/min, the VCFSW joint with integral surface is obtained, which results from sufficient frictional heat that can soften, smash, and stir compensation strip and BM and then attains better material flow and mixture of two material wells (Fig. 3b). As the welding speed increases to 100 mm/min, the surface of joint becomes rough. This is because the increase of welding speed decreases frictional heat, which causes welded material that is difficult to be plastic state due to the decrease of heat input (Fig. 3c). When the welding speeds increase to 150 and 200 mm/min, the obvious defect marked by dashed line forms in the surface of joint, where the stress concentration phenomenon easily appears during tensile test, as revealed in Fig. 3d, e, f. In this study, this defect is named scar. During VCFSW process, rotational tool contacts with both BM and compensation strip. With the increase of welding speed, the heat input gradually decreases, which is hard to make materials reach sufficient plastic state and then results in worse material flow, generating irregular flow [21]. With the advancement of rotational tool, the force endured by rotational tool is changeful because of irregular material flow, which may cause the vibration of rotational tool through the thickness direction, leading to the formation of scar defect.

As welding speed further increases to 300 mm/min, it can be observed that the scar defect close to the starting point of VCFSW is worse than 150 and 200 mm/min, as displayed in Fig. 3f. Moreover, even more serious is that

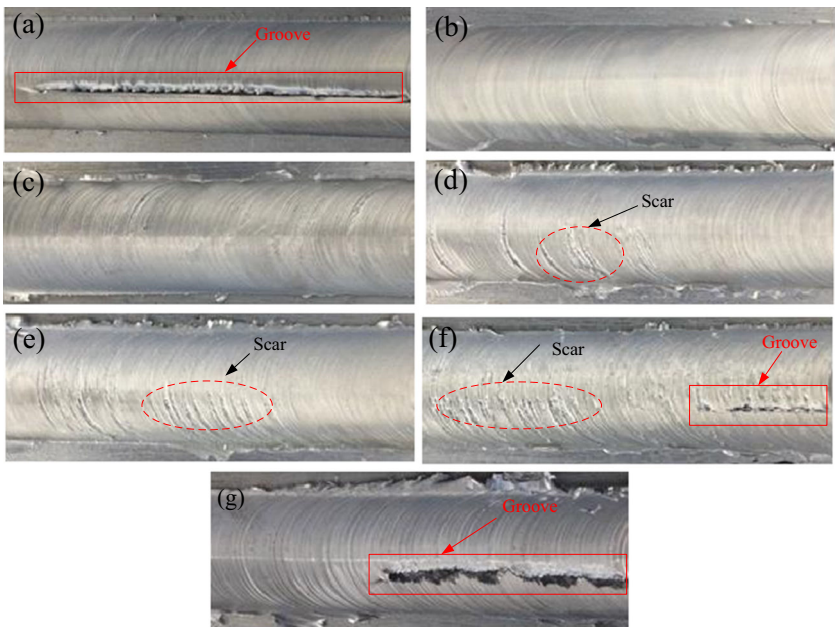

Fig. 3 Surface formation of joints obtained under different welding processes: **a** 1-mm gap and no compensation material; width of 1-mm strip at the welding speeds of **b** 50, **c** 100, **d** 150, **e** 200, and **f** 300 mm/min; **g** width of 1.5-mm strip at the welding speed of 50 mm/min

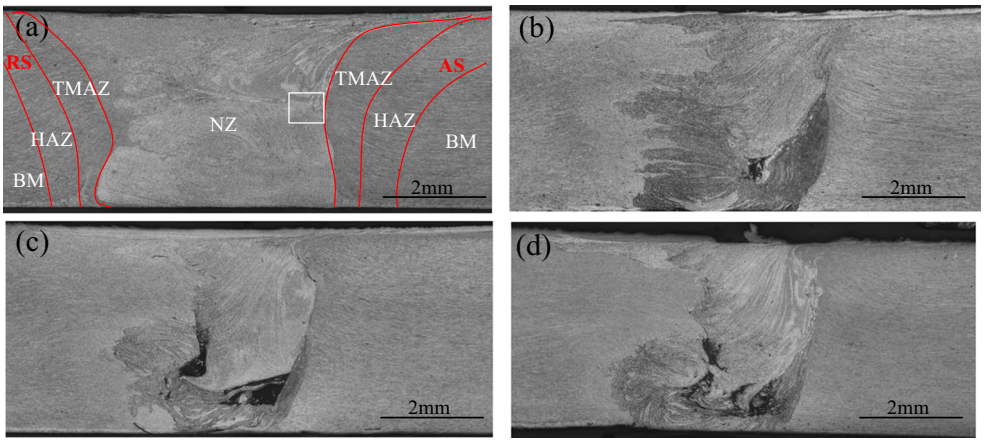

Fig. 4 Macrostructures of joints under different welding speeds: **a** 50, **b** 100, **c** 150, and **d** 200 mm/min

groove defect forms distance away from the starting point. During VCFSW process, before the advancement of rotational tool, the frictional heat generated at the dwelling stage can preheat compensation strip and BM close to the starting point. With the advancement of rotational tool, heat input per unit length gradually decreases owing to the reduction of preheating effect so that compensation strip and BM are difficult to be broken into pieces and then mix, which leads to inadequate material flow, resulting in the formation of groove defect.

To study effective width of gap eliminated by VCFSW for 7N01 aluminum alloy, VCFSW experiment under the strip of 1.5 mm width was performed. Meanwhile, surface formation of the joint is shown in Fig. 3g under the welding speed of 50 mm/min and rotational velocity of 2000 rpm. It is seen that the groove defect appears in the NZ. During VCFSW process, frictional heat is related to effective contact area between rotational tool and workpieces consisting of BM and compensation strip. As the strip width increases from 1 to 1.5 mm, the effective contact area between rotational tool and BM decreases, while the contact area between rotational tool and compensation strip increases. For FSW process, it is easy to make peak temperature reach 90 % of the melting temperature of BM [1, 22]. Therefore, the heat input under 1.5 mm width decreases compared with 1 mm width, which, in turn, causes higher flow stress and worse material flow resulting in the formation of groove defect. Interestingly, in our pre-experiment, it was not yet found that the groove defect formed in the VCFSW of 6061 alloy with 1.5 mm width strip. It is possibly because that the hardness of 7N01 alloy is higher than that of 6061 alloy. During VCFSW of 7N01 alloy process, the decrease of heat input per unit resulted from the increase of strip width may lead to bigger flow stress and then obtain worse material flow compared with 6061 alloy [23]. Therefore, it is concluded that decreasing welding speed increases frictional heat and then obtains better material flow, which is beneficial to surface formation of VCFSW joint of 7N01 alloy.

3.2 Macrostructure and microstructure of joint

Figure 4 reveals macrostructures of VCFSW joints in cross section under different welding speeds. During traditional FSW process, with the advancement of rotational tool, a cavity occurs instantaneously behind rotational pin. Under the combination of tool rotation and translation, the material in the front of the pin is transferred to the back of the pin, completing the filling of cavity. Figure 4a indicates that defect-free joint is attained at the welding speed of 50 mm/min. Meanwhile, the NZ is characterized by intercalation lamellae structure consisting of black and white bands, which is shown in Fig. 4a. The intercalation lamellae structure is also reported by dissimilar FSW of aluminum and magnesium alloy, which is attributed to the different etching response to Keller's reagent [17, 24, 25]. In order to further understand the black and white bands, the EDX experiment of special positions was carried out, as marked in Fig. 5. Because 2024 alloy is Al–Cu alloy and 7N01 alloy is Al–Zn alloy, Al, Cu, and Zn are mainly detected to distinguish the black and white bands. The results of elemental analysis are revealed in Table 2. It is seen that the

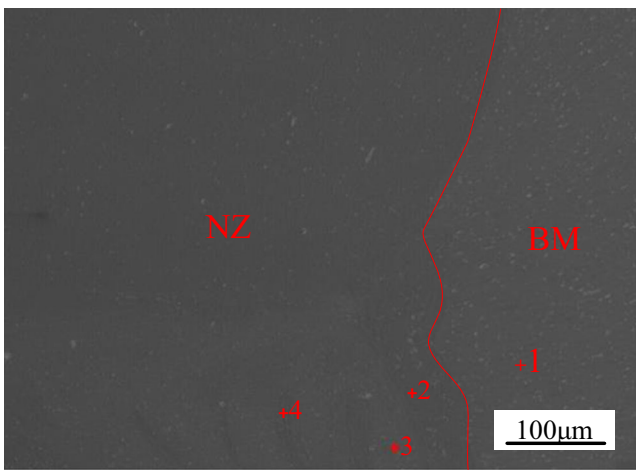

Fig. 5 SEM micrograph taken from the area marked by white square in typical morphology of joint at the welding speed of 50 mm/min in Fig. 4

Table 2 Elemental analysis results of the interface for VCFSW joint of 7N01-T4 alloy

Rotational velocity (rpm)	Welding speed (mm/min)	Width (mm)	Position	Element (wt%)		
				Al	Zn	Cu
2000	50	1	1	95.19	4.63	0.18
			2	95.55	0.19	4.26
			3	95.29	4.56	0.15
			4	95.25	0.23	4.52

wt% of Zn of positions 1 and 3 conform to 7N01 alloy, while the wt% of Cu of positions 2 and 4 accord with 2024 alloy. Therefore, it is verified by EDX that the white band containing positions 1 and 3 is 7N01 alloy as a result of higher Zn content. In the meantime, it is also inferred that the black band including positions 2 and 4 belongs to 2024 alloy owing to higher Cu content [17]. In addition, based on the features of intercalation lamellae structure of VCFSW joint, it could be potentially applied to investigate the material flow behavior in terms of optimizing the shape of rotational tool [25]. Shiri et al. [26] has also stated that inserting metallic foils into the FSW joint could better reveal the material flow during FSW process.

As shown in Fig. 4a, similar to traditional FSW process, the macrostructure of VCFSW joint in cross section is divided into four zones: NZ, thermo-mechanically affected zone (TMAZ), heat-affected zone (HAZ), and BM [1]. VCFSW joint produces obvious difference between TMAZ of advancing side (AS) and TMAZ of retreating side (RS). A sharp interface appears between the TMAZ of AS and NZ, while the interface between the TMAZ of RS and NZ is unclear due to the differences of shear stress and direction of material flow velocity [27]. In this study, because the right-screwed rotational pin rotates anti-clockwise during VCFSW process, the materials around rotational pin flow toward the bottom with the

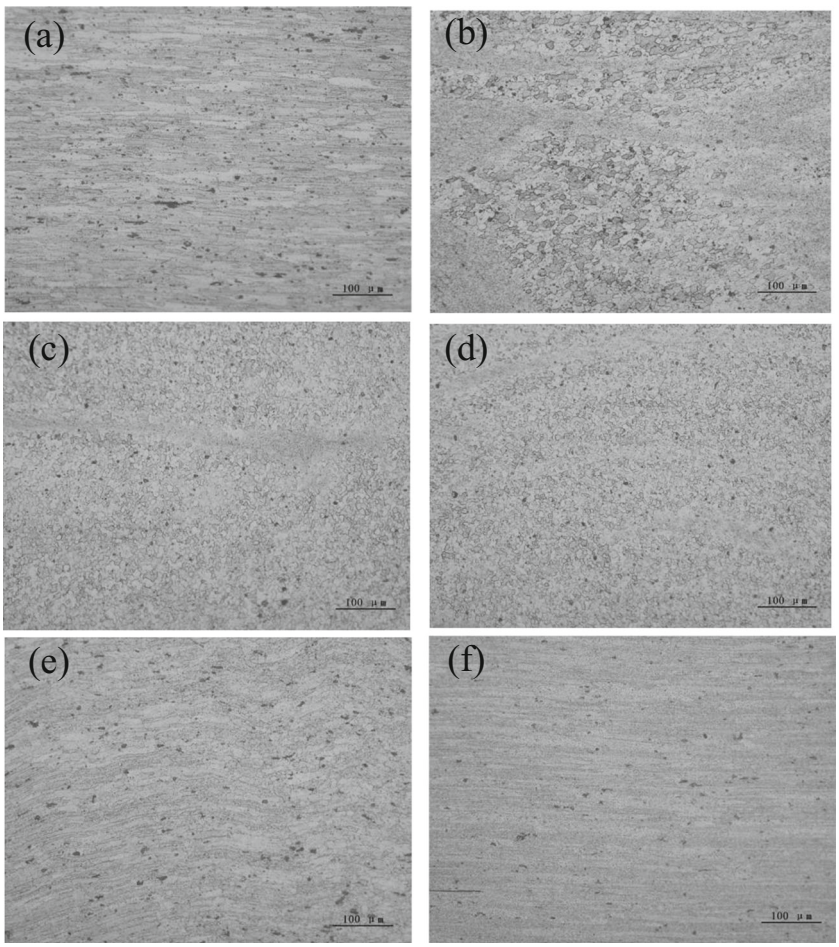

Fig. 6 Microstructures of different positions of joint at the welding speed of 50 mm/min: **a** BM, **b** surface of NZ, **c** middle of NZ, **d** bottom of NZ, **e** TMAZ, and **f** HAZ

rotation of the pin [28]. It is seen that compensation material is accumulated in the bottom of joint rather than the top at the welding speed of 50 mm/min (Fig. 4a). As welding speeds increase from 100 to 200 mm/min, the cavity defect forms in the bottom of joint, as indicated in Fig. 4b–d. As a matter of fact, the formation of welding defect is related to both uneven material flow and volume deficiency of plasticized materials [29]. When the welding speed is 50 mm/min, the defect-free joint is attained, which eliminates volume deficiency factor. Therefore, the formation of cavity defect is attributed to inadequate material flow. When the welding speed increases to 100 mm/min, the heat input per unit length decreases, which causes that rotational tool cannot sufficiently soften, stir, and mix compensation material and BM, leading to the formation of cavity defect (Fig. 4b). The presence of cavity defect diminishes the effective cross-sectional area of joint, which easily results in stress concentration and the decrease of load bearing, deteriorating mechanical property of joint. Moreover, the cavity defect easily becomes crack initiation under large tension stress. With further increasing welding speed to 150 and 200 mm/min, the peak temperature decreases, which results in worse material flow and less time to mix two materials, forming the cavity defect with bigger size compared with 100 mm/min, as observed in Fig. 4c, d. Therefore, the conclusion can be obtained that lower welding speed is propitious to higher peak temperature and gives more time for the tool to soften, stir, and mix two materials, obtaining defect-free joint.

Microstructures of different positions of VCFSW joint at the welding speed of 50 mm/min are presented in Fig. 6. BM displays the elongated lath-shaped grains because of the rolling process (Fig. 6a). NZ is characterized by fine and equiaxed microstructures of 2024 alloy and 7N01 alloy, which is due to dynamic recrystallization resulted from high peak temperature and stain rate. Microstructures of different positions of NZ through the thickness direction are displayed in Fig. 6b–d, which locate in the surface, middle, and bottom of NZ, respectively. It can be seen that the grain size gradually decreases from the surface to bottom of NZ. During traditional VCFSW process, frictional heat is generated by the shoulder and the pin, while the amount of frictional heat produced by shoulder is greatly larger than that by pin, which gives sufficient heat and time for microstructures of surface to grow [25, 30]. In addition, the material in the surface gets in touch with atmosphere, and heat convection is the main way to lose heat. Therefore, the grain size in the surface of NZ reaches approximately 13 μm. However, the material in the bottom contacts with backing plate made of steel, and quick heat loss happens owing to heat conduction, which is favorable to obtain smaller size grains (average value of 6 μm) and then obtains higher hardness. Additionally, the frictional heat experienced by materials in the middle of NZ is far less than surface, which leads to formation of grain size with average value of 7 μm. TMAZ is featured by deformed and elongated grains suffered from

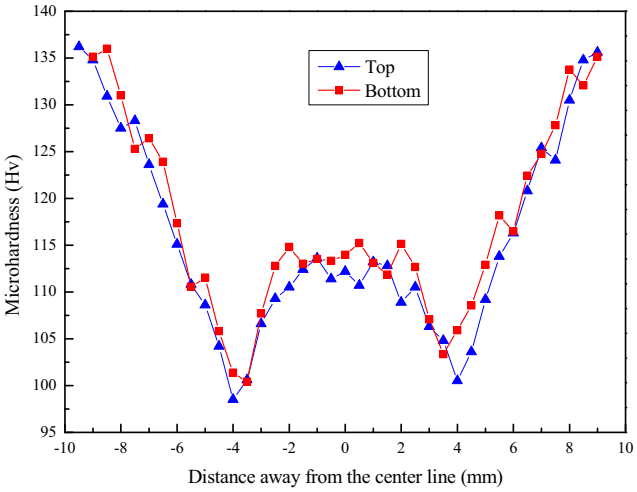

Fig. 7 Microhardness distribution through the thickness direction of joint at the welding speed of 50 mm/min

thermal cycle and mechanical effects, as shown in Fig. 6e. HAZ only experiences thermal cycle without plastic deformation, which is filled with coarsened grains compared with BM (Fig. 6f).

3.3 Hardness distribution

In order to investigate the effect of compensation material on hardness of VCFSW joint, microhardness distribution in the top and bottom of the defect-free joint obtained using the welding speed of 50 mm/min is mainly discussed, as exhibited in Fig. 7. Therein, microhardness distribution in the top and bottom is 1 and 3 mm to the top surface, respectively. As commonly seen in the traditional FSW, the softening phenomenon is occurred in the VCFSW joint of 7N01 alloy, which is attributed to dissolution, reprecipitation, and coarsening of strengthening precipitates [31, 32]. The average value of NZ

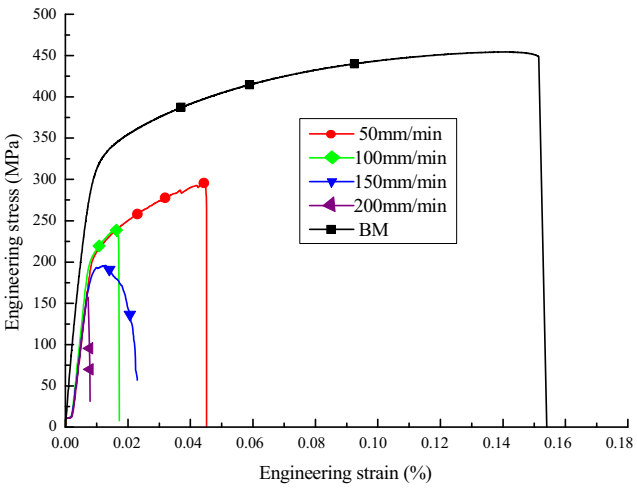

Fig. 8 Engineering stress and strain of BM and joints under different welding speeds

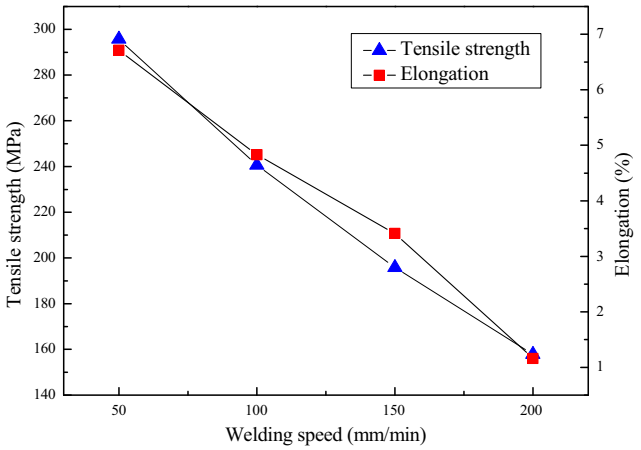

Fig. 9 Tensile strength and elongation of joints under different welding speeds

is lower than BM but higher than that of HAZ and TMAZ, which is due to the fine and equaixed microstructures resulted from dynamic recrystallization of NZ. Therefore, the hardness distribution of joint presents typical "W" shape. To be worthy of attention, the addition of compensation material does not result in an uneven hardness distribution of NZ, indicating the rationality of compensation material that can better mix with BM. It is observed that through the thickness direction, the hardness in the bottom is slightly higher than that in the top because of the difference of grain size caused by the difference of thermal cycle. Meanwhile, it is seen obviously that the minimum hardness locates in TMAZ, which easily becomes weak region of mechanical property and fractures along TMAZ during tensile test.

3.4 Mechanical property of joint

The experimental results of tensile specimens obtained using different welding speeds are exhibited in Figs. 8 and 9. It is seen that with the increase of welding speed, the tensile strength, and elongation of VCFSW joint decrease (Fig. 9). During conventional FSW process, mechanical properties of joint increase with the increase of welding speed, which is related to some beneficial microstructure effects caused by the fast cooling at higher welding speed for sound joint. However, in this study, the opposite behavior is typically observed, resulting from the presence of internal defects with the increase of welding speed. Therefore, at the welding speed of 50 mm/min and constant rotational velocity of 2000 rpm, the tensile strength and elongation of joint reach maximum values of 295.7 MPa and 6.7 %, equivalent to 66 and 39.4 % of BM, respectively.

During traditional FSW process, welding speed has a significant influence on temperature distribution, peak temperature, and cooling rate, which, in turn, affects joint quality, especially VCFSW process [33]. When welding speed is lower, heat input per unit length rises and higher peak temperature is obtained, which are helpful to attain better material flow behavior and intense mixture of two materials. Moreover, the lower welding speed is beneficial to give much time for heat to transfer and mixture between compensation material and BM during VCFSW process. Therefore, under the welding speed of 50 mm/min, it is easy to obtain sound VCFSW joint. As shown in Fig. 8, the joint at 50 mm/min experiences a short necking, which is same as BM, obtaining better mechanical properties. Meanwhile, the fracture location of VCFSW joint is exhibited in Fig. 10. For traditional FSW joint, it is widely acceptable that the tensile fracture is likely to occur at the defect position or minimum hardness location [34]. Furthermore, in terms of VCFSW process, the degree of mixture of two materials also plays a more significant role in the tensile fracture of joint. In this study, the tensile fracture is influenced by the degree of mixture and minimum hardness location for the sound joint at 50 mm/min. It is observed from Fig. 10b that the fracture location lies in TMAZ rather than NZ, which validates the better mixture of compensation material and BM at 50 mm/min. In addition, the fracture position (TMAZ) is agreement with hardness distribution (Fig. 7). As

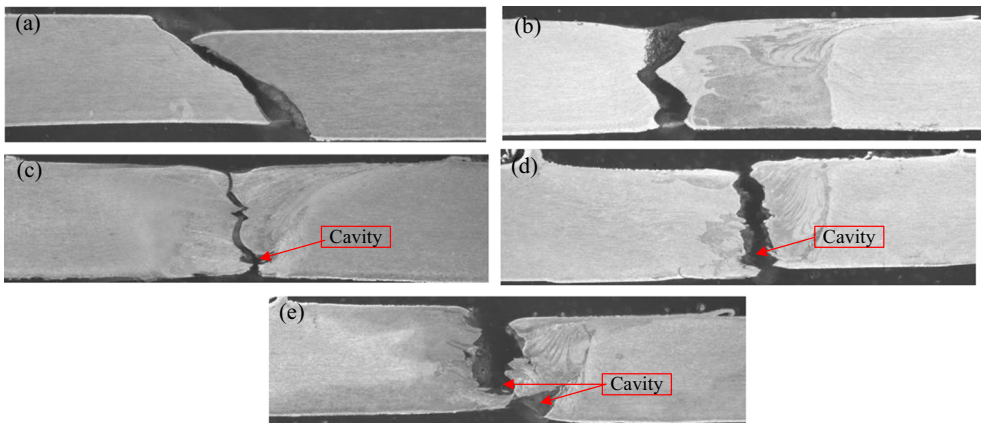

Fig. 10 Fracture position of tensile specimens of BM and joints under different welding speeds: **a** BM, **b** 50, **c** 100, **d** 150, and **e** 200 mm/min

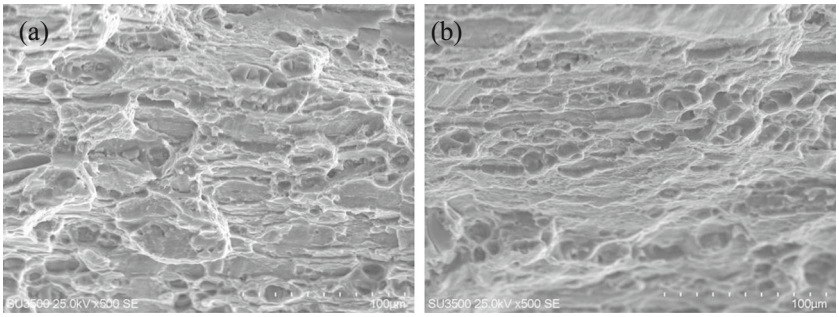

Fig. 11 Fracture surface morphologies of BM and joint at the welding speed of 50 mm/min: **a** BM and **b** 50 mm/min

mentioned above, the increase of welding speed not only decreases heat input per unit length but also results in less time to soften, stir, and mix two materials. However, the sufficient mixture time is more important for VCFSW process. Therefore, the occurrence of cavity defect reduces the degree of mixture in the joints at the 100, 150, and 200 mm/min, deteriorating mechanical properties (Fig.4b–d). Therefore, the fracture of VCFSW joint with cavity defect initiates at the cavity defect and then propagates into NZ, leading to the fracture of joint. In addition, the appearance of cavity also weaken the degree of mixture and mechanical interlock of joint, which is detrimental to load bearing of joint [35].

Figure 11 shows fracture surface morphology of BM and joint obtained at the welding speed of 50 mm/min. It is seen that fracture surface morphology is characteristic by various size dimples, displaying typical ductile fracture. At the welding speed of 50 mm/min, the fracture surface of joint is featured by smaller and shallower dimples compared with BM, which indicates that the joint undergoes plastic deformation, exhibiting good ductility of VCFSW joint. With the increase of welding speed, the cavity defect appears in the joints attained at the welding speeds varying from 100 to 200 mm/min, which always becomes the initiation of fracture. Therefore, fracture surface morphology of these joints is not given.

4 Conclusion

The VCFSW of 7N01-T4 aluminum alloy was successfully performed, and effects of welding speed on formation, microstructures, and mechanical properties of joint were studied. On the basic of present investigation, the following conclusions can be drawn:

1. At the constant rotational velocity of 2000 rpm, the defect-free VCFSW joint with integral surface is attained under the welding speed of 50 mm/min and strip width of 1 mm. The NZ is filled with intercalation lamellae structure composed of black and white bands, which can reveal the material flow behavior used in the optimization of rotational tool.
2. When the strip width is 1.5 mm, it is difficult to obtain sound joint. Decreasing welding speed increases frictional heat and gives sufficient time to mix two materials, which are beneficial to formation of joint.
3. With the increase of welding speed, mechanical properties of joint gradually decrease. The tensile strength and elongation of joint at the welding speed of 50 mm/min and strip width of 1 mm are 295.7 MPa and 6.7 %, up to 66 and 39.4 % of BM, respectively. Meanwhile, the fracture surface morphology shows typical ductile fracture.
4. The hardness distribution presents W curve. The compensation material can mix with BM sufficiently and then obtain well-distributed hardness in the NZ.

Acknowledgments This work is supported by the National Natural Science Foundation of China (No. 51204111), the Natural Science Foundation of Liaoning Province (No. 2013024004 and No. 2014024008), the Project of Science and Technology Department of Liaoning Province (No. 2013222007), and the Aeronautical Science Foundation of China (2014ZE54021).

Reference

1. Mishra RS, Ma ZY (2005) Friction stir welding and processing. Mater Sci Eng R 50:1–78
2. Wan L, Huang YX, Lv ZL, Lv SX, Feng JC (2014) Effect of self-support friction stir welding on microstructure and microhardness of 6082-T6 aluminum. Mater Des 55:197–203
3. Li JQ, Liu HJ (2013) Design of tool system for the external nonrotational shoulder assisted friction stir welding and its experimental validations on 2219-T6 aluminum alloy. Int J Adv Manuf Technol 66(5-8):623–634
4. Liu HJ, Zhao YQ, Hu YY, Chen SC, Lin Z (2015) Microstructural characteristics and mechanical properties of friction stir lap welding joint of alclad 7B04-T74 aluminum alloy. Int J Adv Manuf Technol 78:1415–1425
5. Nandan R, Debroy T, Bhadeshia HKDH (2008) Recent advances in friction-stir welding-process, weldment structure and properties. Prog Mater Sci 53(6):980–1023
6. Kim YG, Fujii H, Tsumura T, Komazaki T, Nakata K (2006) Three defect types in friction stir welding of aluminum die casting alloy. Mater Sci Eng A 415(1):250–254
7. Lombard H, Hattingh DG, Steuwer A, James MN (2008) Optimising FSW process parameters to minimise defects and maximise fatigue life in 5083-H321 aluminium alloy. Eng Fract Mech 75(3):341–354

8. Liu HJ, Zhang HJ (2009) Repair welding process of friction stir welding groove defect. Trans Nonferrous Met Soc China 3:563–567
9. Yao JS, Zhang CJ, Wei W (2012) Repair welding technique for tunnel defects of FSW joints. Aerosp Mater Technol 1:73–76 (in Chinese)
10. Ji SD, Meng XC, Liu JG, Zhang LG, Gao SS (2014) Formation and mechanical properties of stationary shoulder friction stir welded 6005A-T6 aluminum alloy. Mater Des 62:113–117
11. Han B, Huang Y, Lv S, Wan L, Feng J, Fu G (2013) AA7075 bit for repairing AA2219 keyhole by filling friction stir welding. Mater Des 51:25–33
12. Seidel TU, Reynolds AP (2001) Visualisation of the material flow in AA2195 friction stir welds using a marker insert technique. Metall Mater Trans A 32(11):2879–2884
13. Takahara H, Tsujikawa M, Chung SW, Okawa Y, Higashi K, Oki S (2008) Optimization of welding condition for nonlinear friction stir welding. Mater Trans 49:1359–1364
14. Takahara H, Motoyama Y, Tsujikawa M, Oki S, Chuang SW, Higashi K (2007) Allowance of deviation and gap in butt joint on friction stir welding. Adv Mater Res 15:375–380
15. Yang Y, Kalya P, Landers RG, Krishnamurthy K (2008) Automatic gap detection in friction stir butt welding operations. Int J Mach Tool Manuf 48:1161–1169
16. Wanjara P, Monsarrat B, Larose S (2013) Gap tolerance allowance and robotic operational window for friction stir butt welding of AA6061. J Mater Process Technol 213(4):631–640
17. Shultz EF, Cole EG, Smith CB, Zinn MR, Ferrier NJ, Pfefferkorn FE (2010) Effect of compliance and travel angle on friction stir welding with gaps. J Manuf Sci Eng 132(4):041010 (9 pages)
18. Ji SD, Meng XC, Ma L, Lu H, Gao SS (2015) Vertical compensation friction stir welding assisted by external stationary shoulder. Mater Des 68:72–79
19. Rhodes CG, Mahoney MW, Bingel WH, Spurling RA, Bampton CC (1997) Effects of friction stir welding on microstructure of 7075 aluminum. Scripta Mater 36(1):69–75
20. Meng LC, Kang X, Sun YJ, Sun K, Shi QY (2012) Mechanical properties of 7N01 aluminum alloy friction stir welding joint. Trans China Weld Ins 33(2):90–92 (in Chinese)
21. GB/T 2650-2008/ISO 6-9016:2001 (2008). Tensile test method on welded joints. Standardization Administration of the People's Republic of China.
22. Galvão I, Oliveira JC, Loureiro A, Rodrigues DM (2012) Formation and distribution of brittle structures in friction stir welding of aluminium and copper: influence of shoulder geometry. Intermetallics 22:122–128
23. Tang W, Guo X, McClure JC, Numes LE (1998) Heat input and temperature distribution in friction stir welding. J Mater Process Manuf Sci 7:163–172
24. Wang Q (2012) Research on reliability of vehicle chassis welded components of CRH2. Harbin Institute of Technology, Harbin (in chinese)
25. Liu C, Chen DL, Bhole S, Cao X, Jahazi M (2009) Polishing-assisted galvanic corrosion in the dissimilar friction stir welded joint of AZ31 magnesium alloy to 2024 aluminum alloy. Mater Charact 60:370–376
26. Guo JF, Chen HC, Sun CN, Bi G, Sun Z, Wei J (2014) Friction stir welding of dissimilar materials between AA6061 and AA7075 Al alloys effects of process parameters. Mater Des 56:185–192
27. Shiri SG, Sarani A, Hosseini SRE, Roudini G (2013) Diffusion in FSW joints by inserting the metallic foils. J Mater Sci Technol 29(11):1091–1095
28. Li JQ, Liu HJ (2013) Effects of welding speed on microstructures and mechanical properties of AA2219-T6 welded by the reverse dual-rotation friction stir welding. Int J Adv Manuf Technol 68(9-12):2071–2083
29. Ke LM, Pan JL, Xing L, Wang SL (2009) Sucking-extruding theory for the material flow in friction stir welds. queryJ Mech Eng Sci 45(4):89–94 (in chinese)
30. Rose AR, Manisekar K, Balasubramanian V (2012) Influences of welding speed on tensile properties of friction stir welded AZ61A magnesium alloy. J Mater Eng Perform 21(2):257–265
31. Huang YX, Han B, Tian Y, Liu HJ, Lv SX, Feng JC, Leng JS, Li Y (2011) New technique of filling friction stir welding. Sci Technol Weld Join 16:497–501
32. Lee WB, Yeon YM, Jung SB (2003) Evaluation of the microstructure and mechanical properties of friction stir welded 6005 aluminum alloy. Mater Sci Technol 19(11):1513–1518
33. Li D, Yang X, Cui L, He F, Zhang X (2015) Investigation of stationary shoulder friction stir welding of aluminum alloy 7075-T651. J Mater Process Technol 222:391–398
34. Ma YE, Xia ZC, Jiang RR, Li W (2013) Effect of welding parameters on mechanical and fatigue properties of friction stir welded 2198-T8 aluminum–lithium alloy joints. Eng Fract Mech 114:1–11
35. Huang YX, Wan L, Lv SX, Feng JC (2013) Novel design of tool for joining hollow extrusion by friction stir welding. Sci Technol Weld Join 18(3):239–246